





RESEARCH ARTICLE | MARCH 18 2024

High-performance of ZnO/TiO₂ heterostructured thin-film photocatalyst fabricated via atomic layer deposition

Special Collection: [Atomic Layer Deposition \(ALD\)](#)

Ji Young Park ; Jeong Hwan Han ; Byung Joon Choi  

 Check for updates

J. Vac. Sci. Technol. A 42, 032404 (2024)

<https://doi.org/10.1116/6.0003348>



View
Online



Export
Citation

 CrossMark

High-performance of ZnO/TiO₂ heterostructured thin-film photocatalyst fabricated via atomic layer deposition

Cite as: J. Vac. Sci. Technol. A 42, 032404 (2024); doi: 10.1116/6.0003348

Submitted: 4 December 2023 · Accepted: 27 February 2024 ·

Published Online: 18 March 2024



Ji Young Park,  Jeong Hwan Han,  and Byung Joon Choi^{a)} 

AFFILIATIONS

Materials Science and Engineering Department, Seoul National University of Science and Technology, Seoul 01811, South Korea

Note: This paper is part of the 2024 Special Topic Collection on Atomic Layer Deposition (ALD).

^{a)}Author to whom correspondence should be addressed: bjchoi@seoultech.ac.kr

ABSTRACT

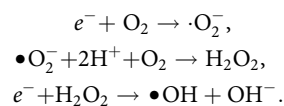
Oxide semiconductor is one of the most promising candidates for photocatalysts due to its light absorption ability, electronic properties, and stability. It is used in various applications such as solar-energy conversion, CO₂ reduction, and water splitting. In this research, ZnO, TiO₂, and ZnO/TiO₂ heterostructured thin films are fabricated via atomic layer deposition (ALD), and their photocatalytic performances are evaluated. The film thickness can be controlled using ALD, and surface reactions can easily occur in thin films owing to the short distances between the active sites and charge carriers. In addition, unlike a powder catalyst, the bilayer photocatalyst is fixed in the solution; therefore, it does not make the solution turbid or disturb the light penetration. Diethylzinc and titanium tetraisopropoxide are used as precursors for Zn and Ti, and the thin films are deposited on soda-lime glass substrates at 150 °C using H₂O as the reactant gas. The photocatalytic activity and stability are evaluated through photodegradation tests using methylene blue aqueous solution. The ZnO single-substance thin film exhibits a high degradation rate, but its performance significantly decreases after three consecutive experiments. The TiO₂ single-substance thin film exhibits a relatively low degradation rate, but high reusability, exhibiting characteristics opposite to that of ZnO. Therefore, a TiO₂ thin film is coated on ZnO to leverage both these advantages. The thin films are heat-treated at 400 °C for 10 min after deposition in a vacuum atmosphere. The surface morphology, crystal structure, and electrical characteristics of the photocatalyst specimens are analyzed through high-resolution scanning electron microscopy, Cs-corrected scanning transmission electron microscopy, and x-ray diffraction analysis. Their photocatalytic performances under ultraviolet (UV) irradiation are measured through UV-visible spectroscopy. The heat-treated ZnO/TiO₂ heterostructured thin film exhibits a photodegradation rate exceeding 80%, with little degeneration after three cycles, indicating enhanced photodegradation performance and stability.

Published under an exclusive license by the AVS. <https://doi.org/10.1116/6.0003348>

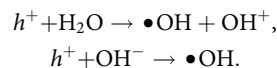
I. INTRODUCTION

Oxide semiconductor photocatalysts have recently attracted attention owing to their great potential for various applications such as solar-energy conversion and water purification.^{1,2} Figure 1 shows the fundamental mechanism of a photocatalytic reaction. When a photocatalyst is exposed to light energy exceeding its bandgap energy, electron-hole pairs are generated on its surface. When reactive oxygen species such as H₂O₂ and OH⁻ radicals are generated through a redox reaction, they decompose the organic pollutants into CO₂, H₂O, and salts.³ The chemical reactions are provided below:

Oxidation reaction:



Reduction reaction:



Since photocatalytic reaction works by the redox process, it is useful to design photocatalysis by coupling two different

19 March 2024 01:05:35

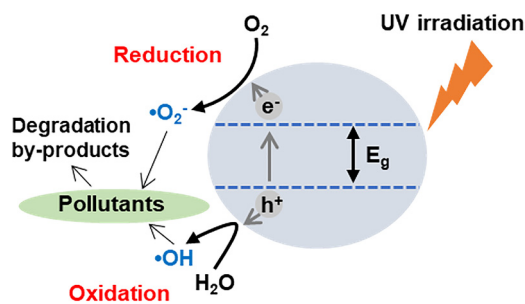


FIG. 1. Schematic diagram of the photocatalytic reaction.

semiconductor materials to generate more electron-hole pairs. A bilayer-structured photocatalyst has various advantages. (1) Owing to the short charge-transport distance to the material surface, it exhibits high photocatalytic performance. (2) The large specific surface area provides effective reactive sites.⁴ (3) Unlike powders and rods, it does not make the solution murky; thus, the photocatalysis always occurs under full irradiation.

In this study, atomic layer deposition (ALD) has been adopted to fabricate a bilayer photocatalyst. ALD is a promising technology for thin-film deposition and is used to deposit conformal nanoscale thin films on substrates of various substances and forms; thus, it is widely adopted in many fields, such as nanoelectronics, displays, batteries, and quantum technologies.^{5–8} It is an exceptional method for depositing an accurate thickness of thin-film stacks with high uniformity. ZnO, TiO₂, and ZnO/TiO₂ heterostructured thin films are fabricated and their film properties as well as photocatalytic performances are researched. ZnO is a semiconductor material with a wide bandgap energy of approximately 3.27 eV. Its low cost and eco-friendly properties make it suitable as a photocatalyst.^{9,10} TiO₂ has a bandgap similar to that of ZnO (approximately 3.0–3.2 eV) and is also nontoxic. Further, it has a high melting point, which makes it thermally stable and difficult to dissolve.^{11–14} Figure 2 shows the charge-transfer process at the ZnO and TiO₂ heterojunction.¹⁵ A main disadvantage of using ZnO as a

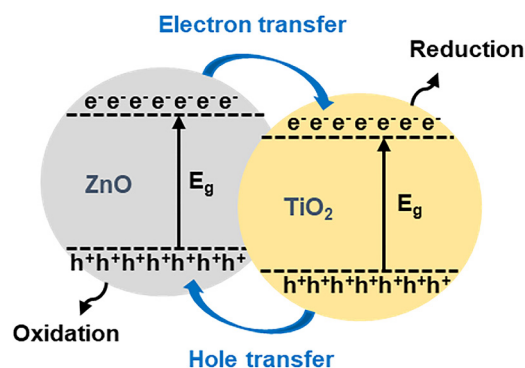


FIG. 2. Mechanism of charge transfer at the ZnO–TiO₂ heterojunction.

photocatalyst is that the electron-hole pairs recombine easily.^{16,17} In order to increase the photocatalytic performance and extend the lifetime, it is important to generate electron-hole pairs quickly while preventing recombination. A heterojunction of different bonded materials with aligned band structures can provide enhanced photocatalytic activity.^{18–21} When two semiconductors with different Fermi energy levels are in close contact, the electrons in the semiconductor with higher energy levels flow to the other semiconductor, reducing the total energy of the system. As a result, net charges accumulate at the interface, lowering the higher Fermi energy level and vice versa. The net charge flow stops when the electrochemical potentials of the two semiconductors become equal and band alignment occurs. When ZnO and TiO₂ are combined, the charge carriers move simultaneously; electrons move from ZnO to the conduction band of TiO₂, which has a relatively lower Fermi energy than that of ZnO, and holes move from TiO₂ to the valence band of ZnO, which has lower Fermi energy than that of TiO₂. This greatly promotes the generation of electron-hole pairs, compared to the cases with a single substance only. The photocatalytic performance can then be improved through the surface and interfacial reactions.^{22–26} In this study, the ZnO/TiO₂ structure is designed to induce high photostability during surface reaction. It is fabricated by ALD to produce ultrathin film based photocatalyst with high photocatalytic activity and long lifetime.

II. EXPERIMENT

In this work, thin films were grown by thermal ALD (Atomic-Shell, CN-1 Co., Korea). The base pressure of the reactor was set at 3×10^{-2} Torr. N₂ gas at a flow rate of 100 SCCM was used to purge reaction products and the process pressure was set as 1.1 Torr. Diethylzinc (DEZ, Lake Materials Co., Korea) and titanium tetraisopropoxide (TTIP, ICHEMS Co., Korea) were used as the precursors of Zn and Ti, and H₂O was used as the reactant gas. The same temperature was applied to ZnO and TiO₂ deposition; a temperature was set to 150 °C with a substrate temperature of 141 °C. The temperature of the precursor was 70 °C for TTIP and 25 °C for DEZ and H₂O. The temperature of the source line was set to 80 °C for TTIP and DEZ, and 100 °C for H₂O. Soda-lime glass (CORNING 2947, 25 × 25 mm²) was used as the substrate. The substrates were first wiped with ethanol and then ultrasonically cleaned with isopropyl alcohol and de-ionized water for 5 min each.²⁷ The ZnO and TiO₂ thin-film deposition processes are described below.¹⁰ For ZnO ALD: DEZ dosing 0.2 s—N₂ purge 15 s—H₂O dosing 0.1 s—N₂ purge 15 s; for TiO₂ ALD: TTIP dosing 0.4 s—N₂ purge 30 s—H₂O dosing 0.5 s—N₂ purge 30 s. The growth per cycle was 0.28 and 0.051 nm/cycle for ZnO and TiO₂, respectively.

Table I presents the details of the photocatalyst samples. The film thicknesses were measured using an ellipsometer (FS-1, Film Sense, USA). In ellipsometry, the four incident light beams—blue (465 nm), green (525 nm), yellow (590 nm), and red (635 nm)—were used simultaneously. The incident angle was 64.767°, and the Cauchy model was applied to fit the data. ZnO and TiO₂ thin films of 20 nm thickness are referred to as Z and T, respectively. The heterojunction samples Z/T10 and Z/T3 correspond to 10-nm and 3-nm-thick TiO₂ films coated on 20-nm-thick ZnO films. Heat

19 March 2024, 01:05:35

TABLE I. Thin-film thickness and heat-treatment details of photocatalyst samples.

| Sample | Thickness (nm) | | Heat treatment |
|---------|----------------|------------------|----------------|
| | ZnO | TiO ₂ | |
| Z | 20 | — | X |
| Z-A | 20 | — | O |
| T | — | 20 | X |
| T-A | — | 20 | O |
| Z/T10 | 20 | 10 | X |
| Z/T10-A | 20 | 10 | O |
| Z/T3 | 20 | 3 | X |
| Z/T3-A | 20 | 3 | O |

treatment was conducted on the four samples in vacuum at 400 °C for 10 min using rapid thermal treatment equipment (REAL RTP/100, Ultech, Korea) and the corresponding sample names are affixed with “-A.”

The cross-sectional images of the surface and crystallographic properties of the thin films were analyzed through high-resolution field-emission scanning electron microscopy (HR-FESEM, SU8010, Hitachi, Japan), Cs-corrected scanning transmission electron microscopy (Cs-STEM, NEO ARM, JEOL, Japan), and x-ray diffraction (XRD, Dmax2500/PC, Rigaku, Japan). In the HR-FESEM analysis, the accelerating voltage was 10 kV and the working distance of 4.7–5.3 mm was used. In XRD analysis, the Cu k_{α} line ($\lambda = 1.54 \text{ \AA}$) was used as the x-ray source. The incident angle was set to 0.5°. The scan speed was 2°/min, the step size was 0.04°, and the scan range was 20°–80°. In the Cs-STEM analysis, the accelerating voltage was 200 kV, the probe current was 1.0 nA, and the convergence angle was 1.5–20 mrad. In the photolysis experiments using a solar simulator (DY TECH, Korea), the intensity of the Xe

lamp used as the light source was set as 400 W/cm² and the distance between the specimen and lamp was 14 cm. Methylene blue (MB) aqueous solution (C₁₆H₁₈N₃SCl·3H₂O) was used after diluting to 10 ppm for 10 ml. The photodegradation test was conducted three times in succession, with one cycle performed every 3 h. After each cycle, the concentration of the solution was measured via ultraviolet–visible (UV–vis, UV-2600i, Shimadzu, Japan) spectroscopy.

III. RESULTS AND DISCUSSION

A. Thin-film analysis

Figure 3 shows the images of the surfaces of the Z and T samples and their annealed versions. Both Z and Z-A are crystallized with elliptical crystal grains, as shown in Figs. 3(a) and 3(b). The average grain size is slightly larger after heat treatment; ~10 nm in Z and ~11.5 nm in Z-A. No grains are found in T and T-A; they are amorphous, as shown in Figs. 3(c) and 3(d).

The crystal structures were investigated via XRD analysis. Figure 4 shows the XRD patterns of T, T-A, Z, Z-A, Z/T10-A, and Z/T3-A. T and T-A are amorphous, and no peaks are detected. Multiple diffraction peaks are observed in the samples that contain ZnO. These peaks correspond to the hexagonal wurtzite structure: (100), (002), (101), (102), (110), (103), and (112). Little difference is observed in the crystallinity before and after annealing. The heterostructured samples Z/T10-A and Z/T3-A also show only diffraction peaks of ZnO, similar to the as-deposited ones. Even after heat treatment, TiO₂ was not crystallized. It seems that higher thermal energy is needed to be crystallized due to the lattice mismatch between TiO₂ and ZnO layers.

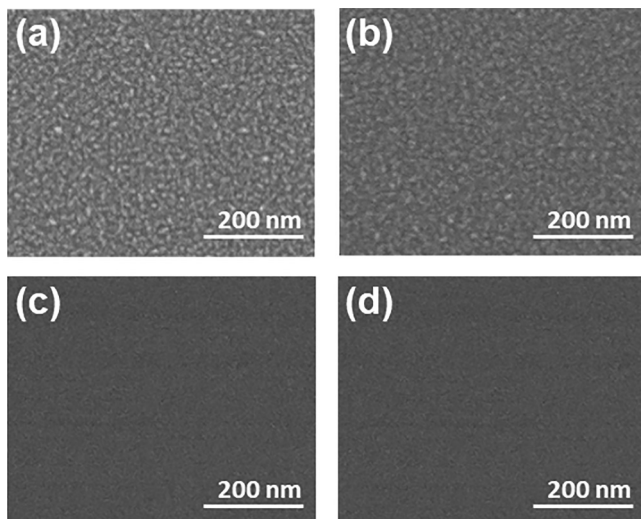


FIG. 3. HRSEM images of (a) Z, (b) Z-A, (c) T, and (d) T-A samples.

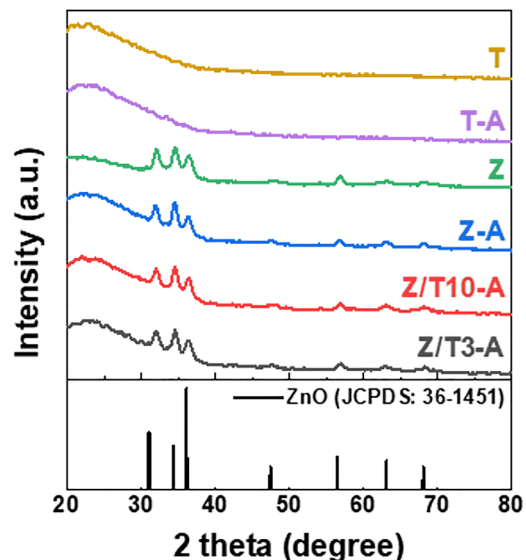


FIG. 4. XRD patterns of single-structured and annealed heterostructured photocatalyst samples.

19 March 2024 01:05:35

The cross-sectional views of the annealed heterostructured thin-film samples were obtained through Cs-STEM. Figure 5 shows the cross-sectional views of the thin-film photocatalyst samples obtained through STEM, EDX spectroscopy, and TEM with FFT pattern analysis. Figures 5(a), 5(b), 5(e), and 5(f) show the images

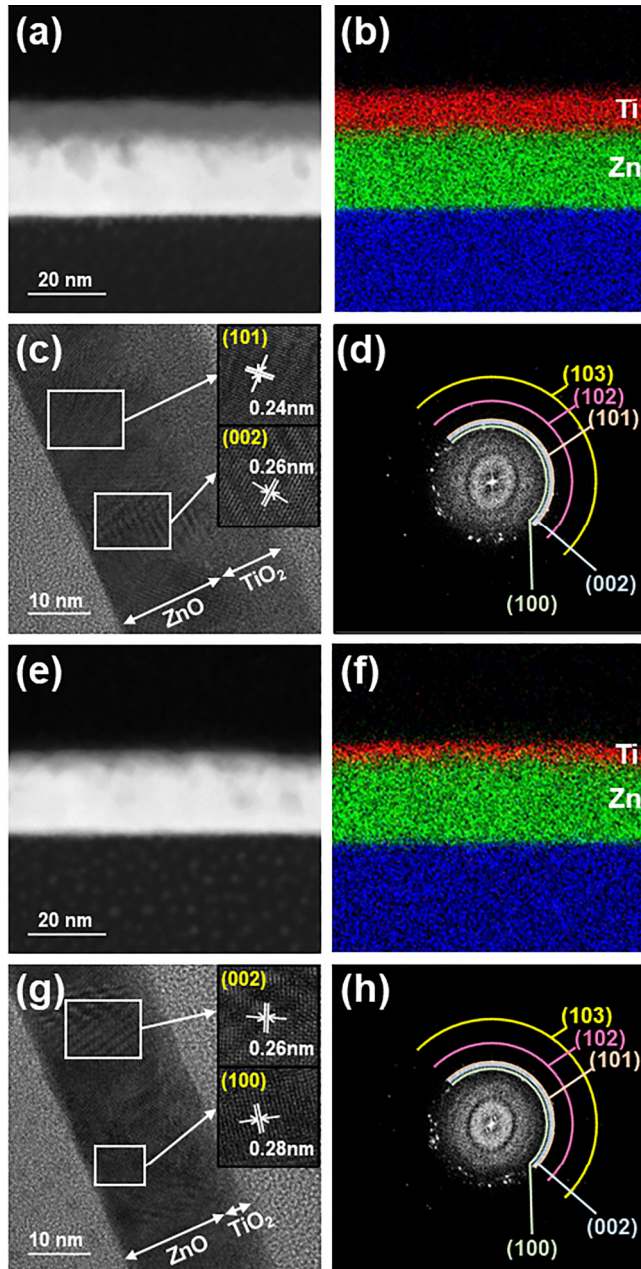


FIG. 5. Cross-sectional STEM image, EDX mapping, TEM image, and FFT pattern of (a)–(d) Z/T10-A and (e)–(h) Z/T3-A.

of ZnO/TiO₂ thin-film structures of Z/T10-A and Z/T3-A, respectively, with the corresponding thicknesses analyzed using an ellipsometer. In Fig. 5(c), the crystallites are aligned along the crystal orientations of (101) and (002) in the ZnO layer, while the TiO₂ layer is confirmed to be amorphous. The FFT patterns in Fig. 5(d) are indexed as (100), (002), (101), (102), and (103), which are confirmed by the XRD patterns. Z/T3-A also shows crystal structures along the (002) and (100) planes in the ZnO layer [Fig. 5(g)] and the FFT patterns show that the same directions with Z/T10-A are fitted [Fig. 5(h)].

The bandgap energy was derived from the Tauc plot calculated using the absorbance spectra obtained via UV-vis spectroscopy.²⁸ Figure 6 shows the Tauc plots and Table II summarizes the calculated bandgap energies of the different samples. TiO₂ has an indirect bandgap structure unlike ZnO, which has a direct bandgap structure. The direct bandgap energy was fitted from the ZnO/TiO₂ structure. T has a higher bandgap energy compared to

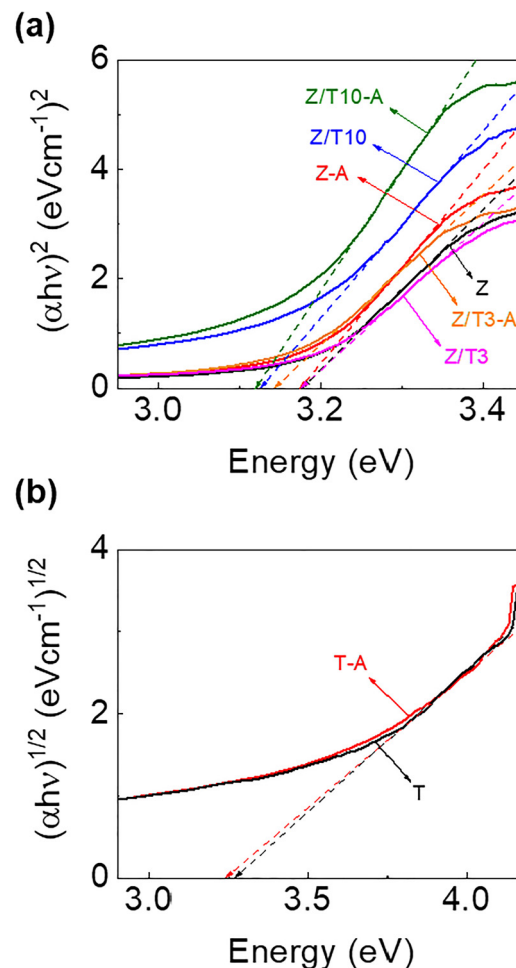


FIG. 6. Tauc plots for (a) direct and (b) indirect bandgap energies of the photocatalysts, derived from the absorbance spectra.

19 March 2024 01:05:35

TABLE II. Bandgap energies derived from Tauc plots of the photocatalysts.

| Sample | Bandgap energy (eV) |
|---------|---------------------|
| Z | 3.18 |
| Z-A | 3.18 |
| T | 3.27 |
| T-A | 3.24 |
| Z/T10 | 3.13 |
| Z/T10-A | 3.12 |
| Z/T3 | 3.18 |
| Z/T3-A | 3.14 |

Z shows the same values before and after annealing, while the other samples decrease slightly following annealing. In the heterostructured photocatalysts, interfacial states could be generated that affects the shift of absorption edge and band alignment, and thus

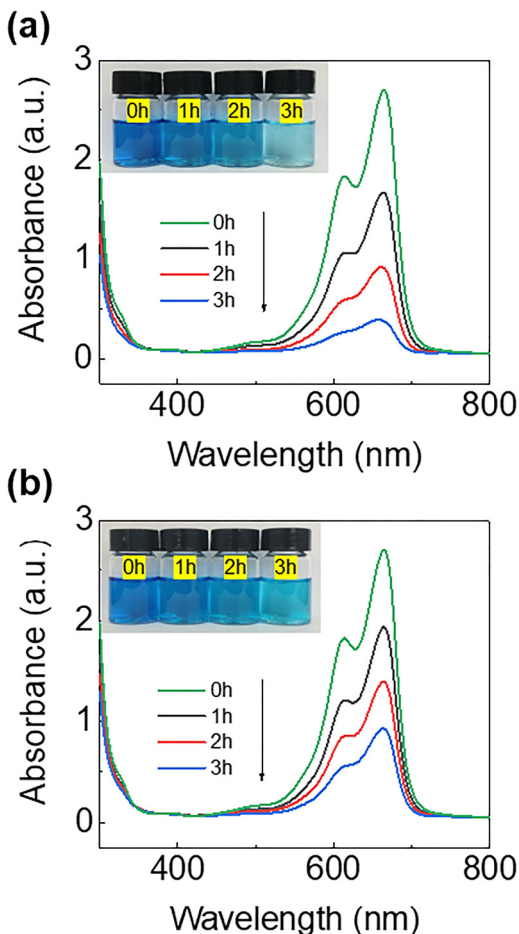


FIG. 7. UV-vis absorbance spectra of MB dye over 3 h of degradation test for (a) Z and (b) T.

the effective bandgap energy becomes lower than that of single-substance photocatalysts.

B. Photocatalytic performance

In order to investigate the photocatalytic properties of the thin-film photocatalyst samples, the photodegradation performance was measured using MB dye. Figures 7(a) and 7(b) present the absorbance spectra of Z and T after 3 h of light irradiation. As shown in Figs. 7(a) and 7(b), the absorption reduction rate of the MB dye over time is larger in Z than in T. After 3 h of light exposure, the absorbance was 0.38 and 0.84 at 664 nm for Z and T, respectively, which confirms that ZnO has greater photolysis efficiency than TiO₂.

Three cycles of successive photodegradation tests were performed, under the same experimental conditions for all the photocatalyst samples, to determine the photocatalytic activity and stability. Figures 8(a) and 8(b) show the photocatalytic activity plot of C/C₀ after three cycles of tests on the single and heterostructured samples. The concentration of the dye under solar irradiation, without photocatalysis, is represented as “MB only” in the figures.

Figure 9 shows the photodegradation efficiency.²⁹ The plot was calculated by using the following formula:

$$\eta = \frac{A_0 - A_t}{A_0} \times 100 (\%), \tag{1}$$

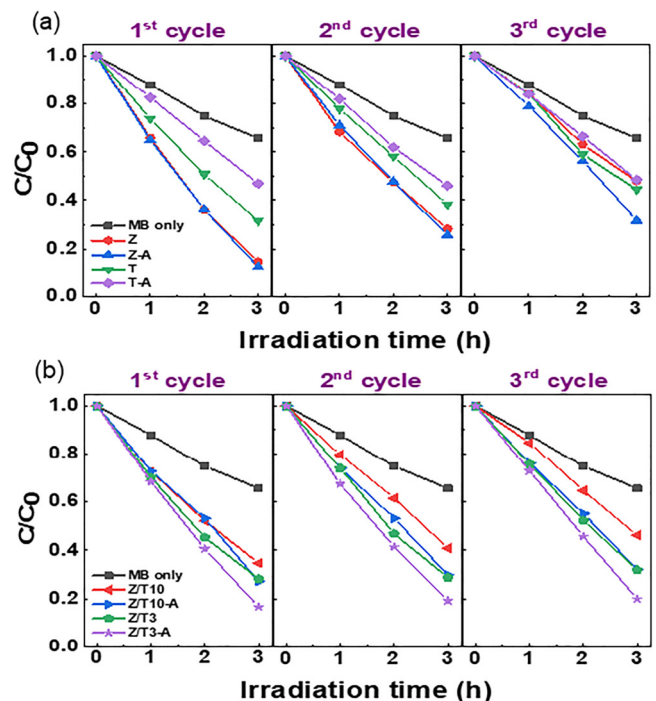


FIG. 8. Photocatalytic activity of (a) single-structured and (b) heterostructured photocatalysts during three cycles of photodegradation tests.

19 March 2024 01:05:35

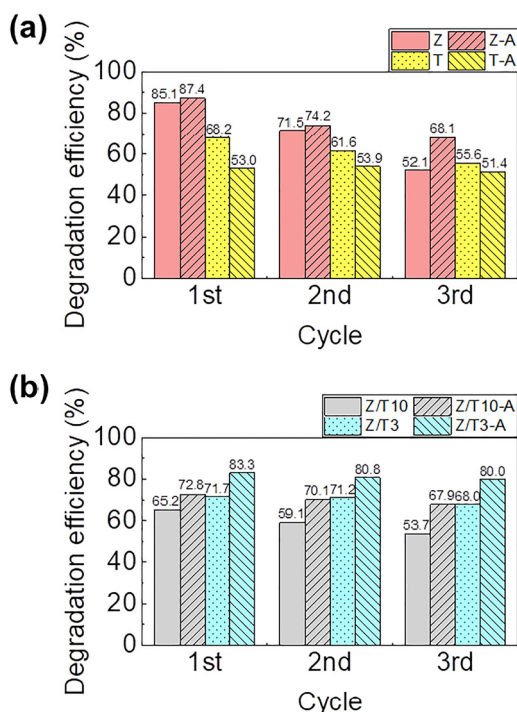


FIG. 9. Degradation efficiency of (a) single-structured and (b) heterostructured photocatalysts during three cycles of photodegradation tests.

where η is the degradation efficiency, A_0 is the absorbance at the beginning, and A_t is the absorbance at t hour.

The photocatalytic activity improves after annealing, except in the case of T. T-A faces further reduction of degradation performance. However, T-A exhibits higher photostability than T, with regard to the lower performance-degradation rate after three cycles. In the first cycle, Z-A shows the best performance, reaching approximately 0.13 of the concentration ratio with 87.37% degradation rate, and T-A records the worst, reaching 0.47 of the concentration ratio with 53% degradation rate. However, after the third cycle, Z-A shows 68.10% efficiency, which decreases by 22.08%, while T-A records 51.40%, which decreases by 3.02%, indicating much higher retention ability than that of Z-A. In conclusion, ZnO exhibits better photocatalytic performance than TiO₂, while its reusability is by far lower because it is vulnerable to photocorrosion. After heat treatment, the photodegradation efficiency of ZnO and stability of TiO₂ increase. As a result, it is possible to combine the advantages of both by fabricating a ZnO/TiO₂ heterostructure. According to Fig. 9(b), the photodegradation efficiency of Z/T3-A decreases by approximately 4.0% during three cycles. Compared to Z-A, which shows the highest photolysis abilities among the single-layer samples, the degradation rate of Z/T3-A is 11.9% higher after three cycles. Z/T10 and Z/T10-A are even worse in terms of both the photocatalytic activity and stability, compared to Z/T3 and Z/T3-A. Sridharan *et al.* recognized that when TiO₂ was coated on ZnO powder, the photocatalytic activity was significantly reduced

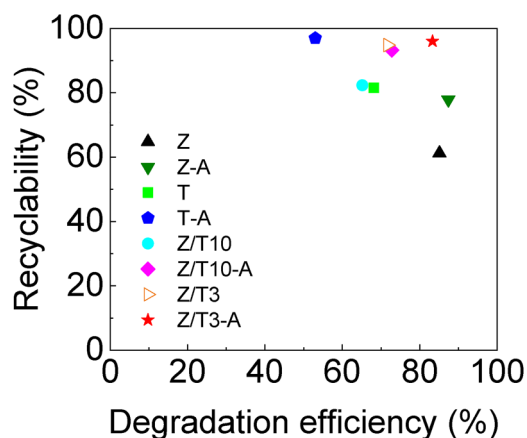


FIG. 10. Degradation efficiency vs recyclability plot of photocatalysts.

while the photostability improved. A thick TiO₂ layer worsened the photoreactivity by increasing the recombination rate of the charge carriers as well as lowering the absorbance of the ZnO core.³⁰ We could minimize the reduction of photoreactivity as well as maximize lifetime by coating TiO₂ ultrathin films on ZnO by ALD.

Figure 10 shows an index that shows the photodegradation rate and lifetime of all photocatalyst samples in this work. Recyclability shows the retention ability of photodegradation efficiency and it is derived by the following formula:

$$\text{Recyclability} = 100 - \frac{\eta(1\text{st cycle}) - \eta(3\text{rd cycle})}{\eta(1\text{st cycle})} (\%). \quad (2)$$

Z/T3-A shows the best photocatalytic properties regarding photoreactivity and stability. Sapkal *et al.* fabricated ZnO, TiO₂, and ZnO/TiO₂ photocatalysts using the spray pyrolysis at 470 °C and found that the ZnO/TiO₂ catalyst had the highest degradation activity. Interestingly, the activity increased as the thickness of the TiO₂ layer increased, which contradicts the findings of our results, possibly due to differences in TiO₂ crystallization.¹⁷ Butalid *et al.* also studied ZnO/TiO₂ photocatalysts fabricated through magnetron sputtering and thermal oxidation on glass substrates. The bare ZnO sample exhibited the highest degradation, while in the case of heterojunction, the efficiency improved with higher ZnO content. The study also observed a decrease in dissolved Zn²⁺ ions during the cycle test, indicating enhanced reusability with a TiO₂ coating similar to our research, supporting the high photocatalytic activity of ZnO and the benefits of coating with TiO₂.²⁶

IV. SUMMARY AND CONCLUSIONS

ZnO and TiO₂ single-layer and ZnO/TiO₂ heterostructured thin-film photocatalysts were grown via ALD. Unlike conventional methods (sputter, spray pyrolysis, dip coating, etc.), ALD is the most powerful method for depositing uniform thin films at the nanoscale. The thin-film properties as well as photocatalytic performances of single, bilayer, and annealed samples were investigated.

19 March 2024 01:05:35

The ZnO/TiO₂ heterojunction exhibited lower direct bandgap energy than each single layer, resulting in enhanced surface reactivity under UV irradiation. Photodegradation experiments using MB dye confirmed that ZnO had high photoreactivity while TiO₂ had high photostability. When single-structured and heterostructured photocatalysts were heat treated, both the degradation efficiency and stability increased, except in the case of T. The Z/T3-A sample showed the best performance, presenting a degradation efficiency of 80% or higher as well as the highest lifetime, during the three-cycle test. By coating 3 nm of TiO₂ thin films on ZnO using ALD, both photocatalytic advantages—stability and reactivity—could be maximized simultaneously. Further, we anticipate the expansion of photocatalyst with the ZnO/TiO₂ coating layer. The heterostructured thin film photocatalyst can be deposited on any other substrates such as powders and nanorods, applying a great advantage of the ALD process and this photocatalysis could be widely used in antibacterial action, degradation of organic materials, and water purification.^{31,32}

ACKNOWLEDGMENTS

This work was supported by the National Research Foundation of Korea (NRF) grant funded by the Korea Government (MSIT) (Nos. 2022R1A4A5033917 and 2023R1A2C1006831).

AUTHOR DECLARATIONS

Conflict of Interest

The authors have no conflicts to disclose.

Author Contributions

Ji Young Park: Conceptualization (equal); Formal analysis (lead); Methodology (lead); Visualization (lead); Writing – original draft (lead); Writing – review & editing (equal). **Jeong Hwan Han:** Conceptualization (supporting); Writing – original draft (supporting); Writing – review & editing (supporting). **Byung Joon Choi:** Conceptualization (supporting); Supervision (lead); Writing – original draft (supporting); Writing – review & editing (equal).

DATA AVAILABILITY

The data support the findings of this study are available from the corresponding author upon reasonable request.

REFERENCES

¹F. Zhang, X. Wang, H. Liu, C. Liu, Y. Wan, Y. Long, and Z. Cai, *Appl. Sci.* **9**, 2489 (2019).
²S. C. Shin, B. K. Park, T. M. Chung, and J. H. Han, *Mater. Lett.* **272**, 127868 (2020).

³C. Regmi, B. Joshi, S. K. Ray, G. Gyawali, and R. P. Pandey, *Front. Chem.* **6**, 33 (2018).
⁴Y. Zhao, S. Zhang, R. Shi, G. I. Waterhouse, J. Tang, and T. Zhang, *Mater. Today* **34**, 78 (2020).
⁵H. Kim, M. J. Jung, S. Choi, and B. J. Choi, *Mater. Today Commun.* **25**, 101265 (2020).
⁶E. Jang, K. Sridharan, Y. M. Park, and T. J. Park, *Chem. Eur. J.* **22**, 12022 (2016).
⁷S. Doyle, L. Ryan, M. M. McCarthy, M. Modreanu, M. Schmidt, F. Laffir, I. M. Povey, and M. E. Pemble, *Mater. Adv.* **3**, 2896 (2022).
⁸W. J. Lee, S. Bera, P. K. Song, J. W. Lee, W. Dai, H. C. Kim, C. S. Kim, and S. H. Kwon, *Jpn. J. Appl. Phys.* **58**, 075501 (2019).
⁹K. M. Lee, C. W. Lai, K. S. Ngai, and J. C. Juan, *Water Res.* **88**, 428 (2016).
¹⁰J. Y. Park, Y. B. Weon, M. J. Jung, and B. J. Choi, *Arch. Metall. Mater.* **67**, 1503 (2022).
¹¹J. K. Lee, Y. K. Kim, B. J. Choi, T. M. Chung, and J. H. Han, *Appl. Surf. Sci.* **480**, 1089 (2019).
¹²D. M. King, X. Liang, C. S. Carney, L. F. Hakim, P. Li, and A. W. Weimer, *Adv. Funct. Mater.* **18**, 607 (2008).
¹³H. Zhao, J. Chen, G. Rao, W. Deng, and Y. Li, *Appl. Surf. Sci.* **404**, 49 (2017).
¹⁴J. Guo, H. Van Bui, D. Valdesueiro, S. Yuan, B. Liang, and J. R. Van Ommen, *Nanomaterials* **8**, 61 (2018).
¹⁵K. Siwińska-Stefańska, A. Kubiak, A. Piasecki, J. Goscińska, G. Nowaczyk, S. Jurga, and T. Jesionowski, *Materials* **11**, 841 (2018).
¹⁶M. Nasr, R. Viter, C. Eid, R. Habchi, P. Miele, and M. Bechelany, *Surf. Coat. Technol.* **343**, 24 (2018).
¹⁷R. T. Sapkal, S. S. Shinde, T. R. Waghmode, S. P. Govindwar, K. Y. Rajpure, and C. H. Bhosale, *J. Photochem. Photobiol. B* **110**, 15 (2012).
¹⁸T. Su, Q. Shao, Z. Qin, Z. Guo, and Z. Wu, *ACS Catal.* **8**, 2253 (2018).
¹⁹S. Yuan, J. Mu, R. Mao, Y. Li, Q. Zhang, and H. Wang, *ACS Appl. Mater. Interfaces* **6**, 5719 (2014).
²⁰M. Pérez-González, S. A. Tomás, M. Morales-Luna, M. A. Arvizu, and M. M. Tellez-Cruz, *Thin Solid Films* **594**, 304 (2015).
²¹J. Tian, J. Wang, J. Dai, X. Wang, and Y. Yin, *Surf. Coat. Technol.* **204**, 723 (2009).
²²Z. Wang, Z. Lin, S. Shen, W. Zhong, and S. Cao, *Chin. J. Catal.* **42**, 710 (2021).
²³C. C. Wang, C. Y. Chou, S. R. Yi, and H. D. Chen, *Int. J. Hydrogen Energy* **44**, 28685 (2019).
²⁴J. F. Lei, L. B. Li, X. H. Shen, K. Du, J. Ni, C. J. Liu, and W. S. Li, *Langmuir* **29**, 13975 (2013).
²⁵G. K. Upadhyay, J. K. Rajput, T. K. Pathak, V. Kumar, and L. P. Purohit, *Vacuum* **160**, 154 (2019).
²⁶K. H. Park, G. D. Han, B. J. Kim, E. H. Kang, J. S. Park, J. H. Shim, and H. D. Park, *Ceram. Int.* **45**, 18823 (2019).
²⁷P. Makula, M. Pacia, and W. Macyk, *J. Phys. Chem. Lett.* **9**, 6814 (2018).
²⁸R. J. B. Butalid, A. P. S. Cristobal, A. D. S. Montallana, and M. R. Vasquez Jr, *J. Vac. Sci. Technol. B* **38**, 062205 (2020).
²⁹S. Jayashree and M. Ashokkumar, *Catalysts* **8**, 601 (2018).
³⁰K. Sridharan, E. Jang, Y. M. Park, and T. J. Park, *Chem. Eur. J.* **21**, 19136 (2015).
³¹S. Choi, J. H. Han, and B. J. Choi, *J. Powder Mater.* **26**, 243 (2019).
³²C. Karthikeyan, P. Arunachalam, K. Ramachandran, A. M. Al-Mayouf, and S. Karuppuchamy, *J. Alloys Compd.* **828**, 154281 (2020).

19 March 2024 01:05:35